AIChE

Synthesis of Multiwalled Carbon Nanotubes on Al_2O_3 Supported Ni Catalysts in a Fluidized-Bed

Jun Liu and Andrew T. Harris
Laboratory for Sustainable Technology, School of Chemical and Biomolecular Engineering, Building J01, University of Sydney, NSW 2006, Australia

DOI 10.1002/aic.11974
Published online September 14, 2009 in Wiley InterScience (www.interscience.wiley.com)

Multiwalled carbon nanotubes (MWNTs) were synthesized on Al_2O_3 supported Ni catalysts from C_2H_2 and C_2H_4 feedstocks in a fluidized bed. The influence of the ratio of superficial gas velocity to the minimum fluidization velocity (U/U_{mf}), feedstock type, the ratio of carbon in the total quantity of gas fed to the reactor, reaction temperature, the ratio of hydrogen to carbon in the feed gas, and nickel loading were all investigated. Significantly, the pressure drop across the fluidized-bed increased as the reaction time increased for all experiments, due to the deposition of MWNTs on the catalyst particles. This resulted in substantial changes to the depth and structure of the fluidized bed as the reaction proceeded, significantly altering the bed hydrodynamics. TEM images of the bed materials showed that MWNTs, metal catalysts, and alumina supports were predominant in the product mixture, with some coiled carbon nanotubes as a by-product. © 2009 American Institute of Chemical Engineers *AIChE J*, 56: 102–113, 2010

Keywords: fluidized-bed, chemical vapor deposition, multiwalled carbon nanotubes

Introduction

Carbon nanotubes (CNTs) are allotropes of carbon with extraordinary electrical, mechanical and chemical properties, making them valuable in applications as diverse as advanced materials,[1] field emission devices,[2] biosensors,[3] molecular electronic devices[4] and conceivably many others. Of the three common techniques for CNT synthesis, laser ablation,[5] arc discharge[6] and chemical vapor deposition (CVD),[7,8] the CVD process shows most promise for economically viable and large-scale synthesis.

Two of the commonly used CVD reactor types for CNT synthesis are the fixed and fluidized-bed. The fixed-bed CVD process, where CNTs grow from metal catalysts dispersed on a suitable support in a gaseous hydrocarbon environment, is typically carried out in a horizontal furnace.[7,8] This results in inhomogeneous gas–solid mixing and heat transfer, restricting the capacity of the technique for commercial applications. The fluidized-bed CVD process, where the reaction occurs within a bed of fluidized catalyst particles, is typically performed in a vertical furnace,[9,10] and in many ways is analogous to existing large-scale catalytic cracking techniques for hydrocarbons (e.g., fluidized catalytic cracking), i.e., the fluidized bed technique provides homogenous mixing and heat transfer between gas and solid and is therefore viable for the large-scale manufacture of CNTs. We have previously defined "large-scale" as being at least 1,0000 tonnes of CNTs per plant per year.[11]

In the literature, the most common metal catalyst for CNT synthesis in fluidized-beds is iron, typically supported on alumina or silica substrates.[12] Studies with nickel and cobalt catalysts are less common. Weidenkaff et al.[13] investigated the synthesis of multiwalled carbon nanotubes (MWNTs) on Fe/Al_2O_3 catalysts in a fluidized-bed but undertook only two experiments using Ni/Al_2O_3 and Ni-doped composite catalysts and one experiment using Co/Al_2O_3 catalysts for

Correspondence concerning this article should be addressed to A. T. Harris at a.harris@usyd.edu.au

Table 1. Summary of the Experimental Conditions for CNT Synthesis

Run	Catalyst	Reaction Temperature (°C)	U/U_{mf}	Feed Gas Composition (vol %)	Reaction Time (min)
R1	5% Ni/Al_2O_3	700	1.5	$C_2H_2:H_2:N_2 = 20:20:60$	30
R2	5% Ni/Al_2O_3	700	3	$C_2H_2:H_2:N_2 = 20:20:60$	30
R3	5% Ni/Al_2O_3	700	4.5	$C_2H_2:H_2:N_2 = 20:20:60$	30
R4	5% Ni/Al_2O_3	700	6	$C_2H_2:H_2:N_2 = 20:20:60$	30
R5	5% Ni/Al_2O_3	700	6	$C_2H_4:H_2:N_2 = 20:20:60$	30
R6	5% Ni/Al_2O_3	700	6	$C_2H_2:H_2:N_2 = 5:20:75$	30
R7	5% Ni/Al_2O_3	700	6	$C_2H_2:H_2:N_2 = 10:20:70$	30
R8	5% Ni/Al_2O_3	700	6	$C_2H_2:H_2:N_2 = 30:20:50$	30
R9	5% Ni/Al_2O_3	650	6	$C_2H_2:H_2:N_2 = 20:20:60$	30
R10	5% Ni/Al_2O_3	750	6	$C_2H_2:H_2:N_2 = 20:20:60$	30
R11	5% Ni/Al_2O_3	800	6	$C_2H_2:H_2:N_2 = 20:20:60$	30
R12	5% Ni/Al_2O_3	700	6	$C_2H_2:N_2 = 20:80$	30
R13	5% Ni/Al_2O_3	700	6	$C_2H_2:H_2:N_2 = 20:10:70$	30
R14	5% Ni/Al_2O_3	700	6	$C_2H_2:H_2:N_2 = 20:40:40$	30
R15	10% Ni/Al_2O_3	700	6	$C_2H_2:H_2:N_2 = 20:20:60$	30
R16	20% Ni/Al_2O_3	700	6	$C_2H_2:H_2:N_2 = 20:20:60$	30
R17	40% Ni/Al_2O_3	700	6	$C_2H_2:H_2:N_2 = 20:20:60$	30

comparison. Corrias et al.[14] studied the synthesis of MWNTs in fluidized-beds using Fe/Al_2O_3 catalysts and Venegoni et al.[9] performed a parametric study on MWNT synthesis using Fe/SiO_2 catalysts. More recently, Morancais et al.[15] performed a parametric study on MWNT synthesis using Fe/Al_2O_3 catalysts with a focus on the unpacked bed density by measuring the bed height and weight before and after synthesis. Fe-based fluidized-bed CVD systems for CNT synthesis have also been studied by Wang et al., [10,16] Hao et al.,[17] Hernadi et al.,[18] Qian et al.,[19] Perez-Cabero et al.,[20] Ago et al.,[21] and Mauron et al.[22] However, when the results of these studies are collectively analyzed, no obvious relationship between CNT product properties and synthesis conditions are observed.[11]

For Ni catalysts only Ago et al.[21] and Li et al.[23] have reported the synthesis of SWNTs on MgO and SiO_2-gel substrates, respectively, from methane (CH_4) and Ermakova et al.[24] and Philippe et al.,[12] the synthesis of carbon nanofibers on both Ni/SiO_2 and Ni/Al_2O_3. In addition, Qian et al.[25] reported the synthesis of MWNTs on Ni—Cu/Al_2O_3 from CH_4 in a two-stage fluidized-bed. Individually, these studies have investigated the effects of temperature, carbon source and catalyst type on the yield and/or selectivity of CNTs. However, no single study investigated all of these variables systematically nor attempted to rationalize the results reported in the literature. In this work, our aim was to systematically study all of the major influential variables for the synthesis of MWNTs on Ni/Al_2O_3 catalysts in a fluidized-bed.

We further note that the majority of CNT reports in the literature on the use of fluidized-beds do not give information on the fluidization regime during synthesis; this information is critical to ensure timely and cost-effective scale-up. For example, while Morancais et al.[15] report the use of a pressure sensor to monitor the fluidization behavior during synthesis, they do not report any of this data in their article. Similarly, Corrias et al.[14] report only a single pressure drop profile. Indeed, a review of the literature shows that a systematic pressure drop study during CNT synthesis in fluidized beds has not been reported. Hence, we present pressure drop data for each experiment undertaken for this article, in part to address this deficiency.

Experimental

Nickel/alumina (Ni/Al_2O_3) catalysts were prepared by wet impregnation.[26] This entails dissolving nickel nitrate hexahydrate [$Ni(NO_3)_2{\cdot}6H_2O$] in deionized water and then mixing with calcined Al_2O_3 powders ($d_{32} = 69.2\ \mu m$). This mixture was dried at 60°C for 12 h and then calcined in a muffle furnace at 500°C for 5 h. The resulting powder was free flowing with the same particle size distribution as the alumina substrate.

For CNT synthesis, 100 g of catalyst was loaded into a fluidized-bed reactor constructed from Inconel 601 stainless steel, 52 mm inner diameter and 1000 mm in length, with a 316 stainless steel gas distributor (with a free surface area of 0.3%) located 250 mm from the base.[11] A vertically aligned, three phase electrical furnace was used to maintain the required temperature during synthesis. During each experiment, the catalyst was first heated to 600°C under N_2 (6 L/min) and then reduced under a H_2/N_2 atmosphere ($H_2:N_2 = 20:80$) at a total flow rate of 6 L/min and a temperature of 600°C for 1 h, before the introduction of carbon source gas. The reactor was then heated to the desired temperature under N_2 at 10°C/min. CNT synthesis was performed under a gas mixture comprising $C_2H_2/H_2/N_2$ or $C_2H_4/H_2/N_2$ for 30 min. The gas flow to the reactor was controlled by a series of mass flow controllers and the system pressure drop was measured using pressure sensors at an acquisition frequency of 10 Hz. Following the completion of an experiment, the system was cooled to room temperature under N_2.

Table 1 gives a summary of the experiments undertaken. In experiments R1–R4, the influence of the U/U_{mf} ratio was studied (1.5, 3, 4.5, or 6, respectively), in R4 and R5, the carbon source gas was changed from C_2H_2 to C_2H_4, whereas in R6, R7, R4, and R8, the C_2H_2 ratio in the total gas feed was studied (at 5, 10, 20, or 30%, respectively). In R9, R4, R10, and R11, the reaction temperature (650, 700, 750, or 800°C, respectively), in R12, R13, R4, and R14, the H_2/C_2H_2 ratio (0, 0.5, 1, or 2, respectively), and in R4, R15, R16, and R17 the Ni loading (5, 10, 20 or 40%, respectively).

The reaction products were characterized by SEM (Philips XL 30 CP), laser particle size analysis (Malvern Mastersizer

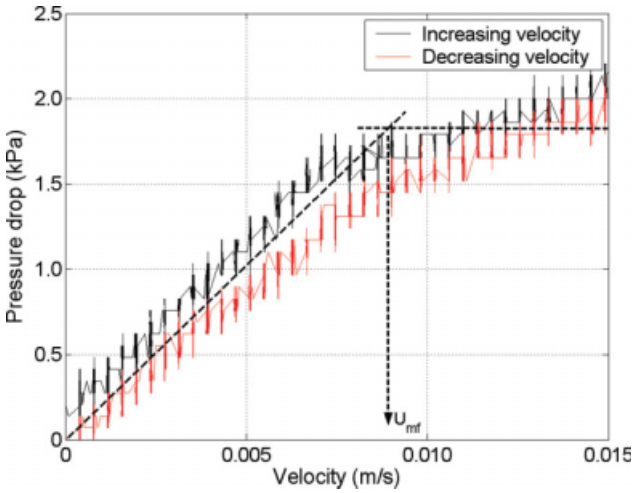

Figure 1. Increasing and decreasing gas velocity vs. pressure drop across a packed bed containing 100 g of calcined Al_2O_3 contacted with N_2 at 700°C.

The dashed line is the trendline for the pressure drop vs. increasing superficial gas velocity. The minimum fluidization velocity is experimentally determined to be 0.009 m/s. [Color figure can be viewed in the online issue, which is available at www.interscience.wiley.com.]

X), thermogravimetric analysis (TGA) (TA SDT Q600), Raman spectroscopy (Renishaw Raman using an Ar^+ ion laser at 514.5 nm), and TEM (Philips CM120 operated at 120 kV).

Results and Discussion

Assessment of the changing fluidization behavior during CNT synthesis

The pressure drop across the gas distributor was first measured in a blank experiment and then subtracted from the measured pressure drop during the synthesis experiments to give the bed pressure drop. Figure 1 is a typical fluidization profile showing pressure drop vs. increasing and decreasing superficial gas velocity, measured using 100 g of calcined Al_2O_3 fluidized with N_2 at 700°C. In Figure 1, the bed pressure drop increases linearly as the superficial gas velocity increases, but when the superficial gas velocity exceeds 0.009 m/s (the minimum fluidization velocity, U_{mf}, corresponding to a gas flowrate of 1.0 L/min in our reactor), the bed pressure drop remains relatively constant; this profile is typical for a bubbling fluidized bed of Group A powders. In practice, it is usual to set the actual gas velocity, U, at somewhere between four and six times U_{mf} to ensure vigorous fluidization.[27,28] Hence, a total gas flow rate of 6.0 L/min was used for all experiments, with the exception of those designed to study the influence of this parameter on the solid carbon yield.

Figures 2a–f shows bed pressure drop profiles during CNT synthesis as a function of time at different U/U_{mf} ratios, carbon source gases, C_2H_2 ratios in the total gas feed, reaction temperatures, H_2/C_2H_2 ratios, and Ni loadings, respectively. Typically, in all experiments, the bed pressure drop increased as reaction time increased; consistent with the observations of Fe-based fluidized-bed systems reported by Corrias et al.[14] and Morancais et al.[15] The increase in bed pressure drop is likely due to two related factors (i) the enlargement of catalyst particles as CNTs grow on their surface and (ii) blockage of the stainless steel distributor caused by local carbon deposition. Figure 3a shows an SEM image of the CNT product (R11), in which separate alumina particles, between 50 and 140 μm in size, are observed. There is little or no agglomeration of the micron-sized alumina particles in the synthesis products. At higher resolution (Figure 3b), entangled CNTs are observed on the surface of the alumina particles. The growth of CNTs on the surface of the catalysts particles is the primary cause of the increase in bed pressure drop during CNT synthesis.

During some experiments, we observed partial blockage of the gas distributor with amorphous carbon deposited during the synthesis reaction, caused by the catalytic decomposition of carbon in the feed gas during contact with the 316 stainless steel distributor. This was despite the very high local gas velocities within the distributor jets. The 316 stainless steel is a Ni/Fe alloy, which has been reported to catalyze the reaction of hydrocarbon gases to amorphous carbon.[29,30] To minimize this phenomena, after each experiment the fluidized bed was unloaded and the holes of the gas distributor physically cleaned. Figure 2 shows that at the starting point of each experiment the measured pressure drop varied between 0 and 2.0 kPa, indicating that this cleaning step was reasonably successful. A review of the literature suggests that stainless steel is most commonly used to construct fluidized-bed reactors for CNT synthesis.[12,14,15,17,31–33] However, our results suggest that for large-scale systems an alternative will likely be required.

Effect of synthesis variables on the bed pressure drop and CNT products

The reaction products were examined using laser particle size analysis to study the catalyst particle enlargement and its influence on the bed pressure drop at different synthesis conditions. Figures 4a–f shows the increase in bed pressure drop during synthesis and the mean particle size (d_{32}) of the reaction products as a function of the U/U_{mf} ratio, carbon source gas type, the C_2H_2 ratio in the total gas feed, reaction temperature, H_2/C_2H_2 ratio and Ni loading, respectively. As expected there is a strong correlation between the primary particle size and the bed pressure drop for all experiments.

TGA was used to determine both the quantity of carbon and its composition in the as-synthesized products (Figure 5). The total weight loss and the temperature at which the rate of weight loss is a maximum during the oxidation of carbon is an indicator of the respective quantities of CNTs and amorphous carbon in the product mix. A review of the literature suggests that weight loss between 300 and 500°C typically corresponds to the oxidation of amorphous carbon (a by-product of the CVD process), whereas the oxidation of MWNTs occurs in the temperature range 500–700°C.[34,35] Therefore, the weight loss region between 400 and 700°C shown in the differential weight loss profiles (Figures 5b, d, f, h, j, l) is suggestive of the oxidation of a mixture of amorphous carbon and MWNTs.

To further differentiate the respective quantities of CNTs and amorphous carbon in the overlapping peaks, a reference

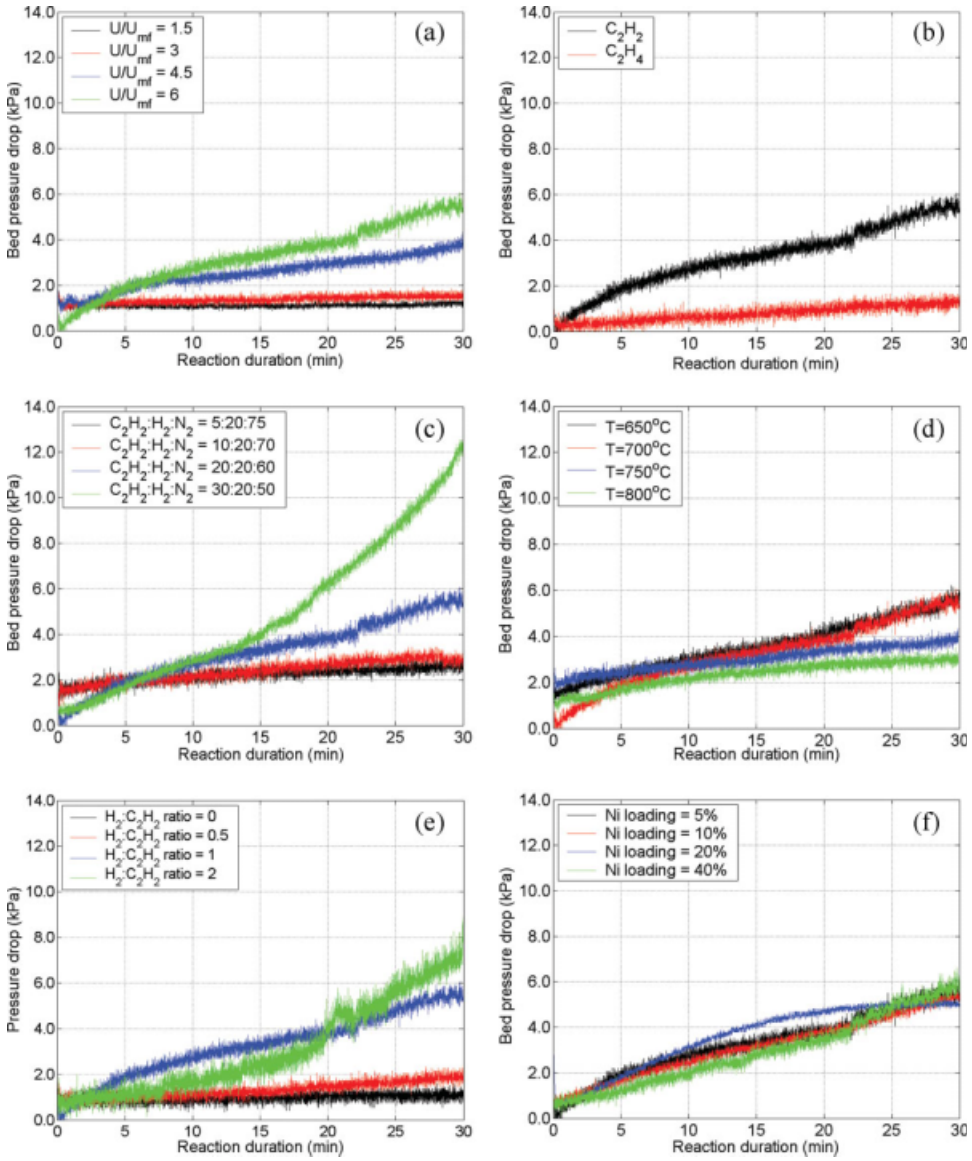

Figure 2. Bed pressure drop profiles for CNT synthesis at various conditions.

The effects of: (a) the ratio of superficial gas velocity to minimum fluidization velocity U/U_{mf} (1.5, 3, 4.5, and 6), (b) carbon source type (C_2H_2 and C_2H_4), (c) the C_2H_2 ratio in the total gas feed (5, 10, 20, and 30%), (d) reaction temperatures (650, 700, 750, and 800°C), (e) H_2/C_2H_2 ratio (0, 0.5, 1, and 2), and (f) Ni loading on Al_2O_3 (5, 10, 20, and 40%) on the bed pressure drop profiles during synthesis were studied. [Color figure can be viewed in the online issue, which is available at www.interscience.wiley.com.]

experiment was performed using Al_2O_3 powders without metal catalysts using a gas mixture of C_2H_2:H_2:N_2 (volume ratio of 20:20:60) at 700°C. This resulted in only amorphous carbon being synthesized on the surface of the Al_2O_3. The oxidization temperature range of this material measured using TGA was between 300 and 500°C. This result was subsequently used to differentiate any overlapping oxidation peaks as follows: weight loss below 500°C was assigned to the oxidation of amorphous carbon, and weight loss above 500°C to the oxidation of CNTs.

Data from the literature further suggests that formation of amorphous carbon as a by-product during fixed-bed CNT synthesis is dependent on several independent variables, e.g., catalyst activity,[36] carbon source flow rate,[37] and the addition of O_2 in the low-temperature CO/Ar plasma technique.[38] Amorphous carbon has also been reported to form on Fe-based catalysts during fluidized-bed CVD synthesis.[20,32,39,40] However, none of these studies reported the effect of synthesis variables on the amorphous carbon yield. Therefore, an additional objective of this work was to determine the quantity of amorphous carbon in the reaction products using TGA in combination of Raman and TEM imaging of the reaction products.

Figures 6a–c show the Raman spectra of the reaction products synthesized with different carbon source gases, reaction temperatures and H_2:C_2H_2 ratios, respectively. Two peaks are clearly visible: (i) a disordered carbon band (D-band) at $\sim$1380 cm^{-1} and (ii) a graphitized band (G-band) at $\sim$1590 cm^{-1}. The D-band typically corresponds to the collective presence of amorphous carbon and defects in the

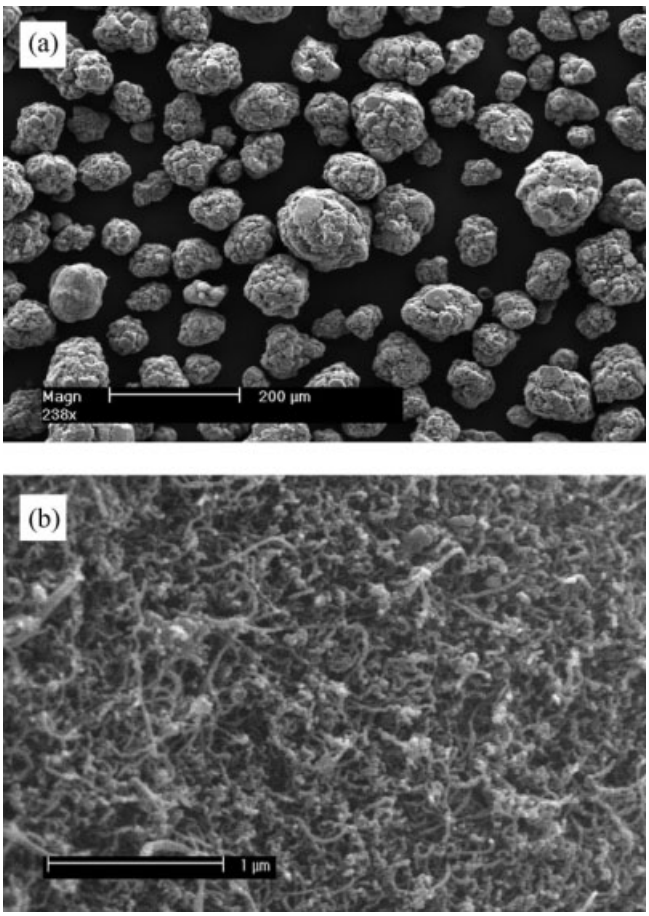

Figure 3. SEM images of the CNT products synthesized on 5% Ni/Al_2O_3 in C_2H_2:H_2:N_2 at the ratio of 20:20:80 at 800°C (R11), (a) low magnification of alumina powders and (b) high magnification of a single particle showing the surface covered with entangled CNTs.

walls of the CNTs, whereas the G-band is characteristic of CNTs (a form of sp^2-bonded crystalline carbon).[22,25,33] The D- and G-band peaks observed in the spectra suggest the presence of CNTs, possibly with some wall defects along with amorphous carbon. Figures 7a–c shows the ratio of D- to G-band intensity (I_D/I_G) calculated from the spectra in Figure 6 as a function of carbon source gas, reaction temperature, and H_2:C_2H_2 ratio, respectively.

Effect of U/U_{mf}

The data in Figure 4a show that the pressure drop across the fluidized bed increased from 0.55 to 5.97 kPa as U/U_{mf} increased from 1.5 to 6. Despite U/U_{mf} exceeding 1 for all of these experiments, i.e., the bed of particles was completely fluidized, indicative of good particle–gas interaction, we observed that higher U/U_{mf} ratios led to much larger bed pressure drops, caused by the increased deposition of carbon on the catalyst particles. This was confirmed by the change in the primary particle size of the reaction products as a function of U/U_{mf} (Figure 4a) and the TGA weight loss data (Figure 5a), which show that both the carbon yield and the temperature at which the maximum rate of weight loss occurred increased as a function of U/U_{mf}. This suggests that there is a critical heat and mass transfer limit in this system, below which the CNT synthesis reaction is suboptimal, despite the bed being fluidized in the traditional sense.

We note, however, that this result is the opposite of Morancais et al.[15] who used a fluidized bed with very similar dimensions to our own reactor, containing 50 g of 2.5 wt % Fe/Al_2O_3 catalyst (d_p = 110 μm) and C_2H_4 as the carbon source. The reaction products were treated with sulphuric acid to dissolve the Fe and Al_2O_3 catalysts before characterization. The TGA results of Morancais et al. showed that the carbon yield decreased from 75 to 51 wt % as the U/U_{mf} ratio increased from 0.78 to 1.1.

It is generally believed that CNT growth via CVD consists of three basic steps: (a) nucleation of active catalyst sites on the substrate surface, (b) extrusion of carbon from the active catalyst site to form tubular structures, and (c) deactivation of catalysts ending CNT growth.[41] Among these, the rate limiting step in the case of C_2H_2 decomposition catalyzed by Ni is likely to be step (b) where the solubility of carbon in Ni is largely dependent on temperature and carbon availability.[41–43] For a large-scale fluidized bed CVD process this means that optimal heat and mass transfer are vital. In this light, the contradiction between the results of Morancais et al.[15] and our own data suggest that the design of fluidized beds for the CNT synthesis requires more detailed study on the optimal heat and mass transfer conditions and the CNT growth mechanism.

In Figure 5b, the differential weight loss profiles show two overlapping peaks comprising a shoulder between 350 and 500°C and a main peak between 500 and 700°C for U/U_{mf} = 1.5, suggesting MWNTs to be the major product and amorphous carbon a by-product. However, at U/U_{mf} = 3, the opposite result was observed; the major peak occurred between 350 and 500°C with a shoulder between 500 and 700°C. This trend reversed again at higher U/U_{mf} values, where there was little amorphous carbon deposited. Thus, the quantity of amorphous carbon increases as the U/U_{mf} ratio increases up to 3, likely caused by early catalyst deactivation, in turn increasing the formation of amorphous carbon. In this case, suboptimal heat and mass transfer between gas and catalyst is the likely cause. However, the quantity of amorphous carbon decreases as the U/U_{mf} ratio increases up to 6, suggesting that heat and mass transfer limitations are reduced at higher U/U_{mf} ratios. Further study is required to confirm these observations.

We also observed an increase in the respective heights of the peaks for amorphous carbon and CNTs as the U/U_{mf} ratio increased from 1.5 to 6, suggesting that the overall quantity of CNTs increased. This is likely due to increased availability of the carbon source as U/U_{mf} increases.

Figures 8a–d shows TEM images of the CNT products synthesized at different U/U_{mf} ratios. These clearly show CNTs interspersed with solid particles forming highly interwoven structures. The particles are most likely metal catalysts and very small crystals of alumina support material. In particular, coiled CNTs are observed in Figures 8a, b, d. In this work, coiled refers to CNTs with a regular coiled structure. To date, no quantitative technique has been developed to distinguish the yield of coiled CNTs from 'straight'

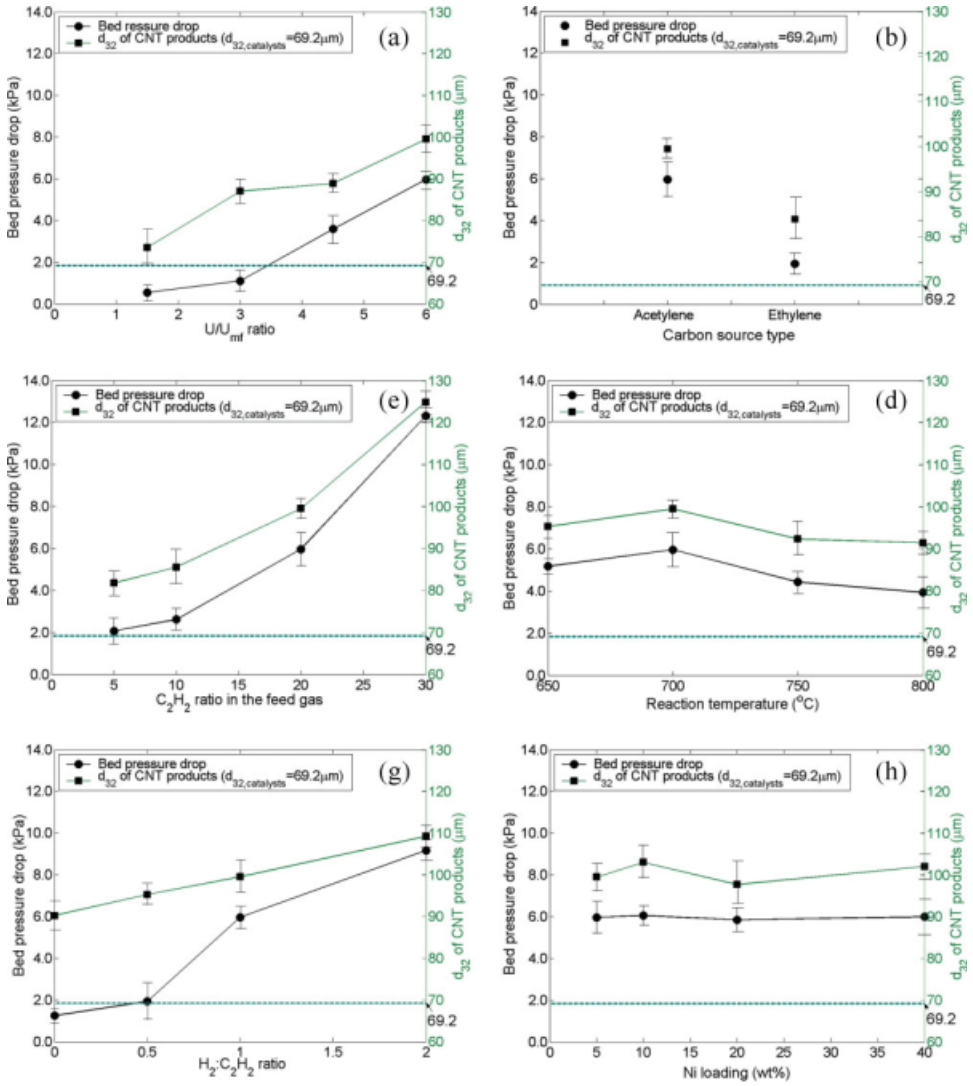

Figure 4. Bed pressure drop during CNT synthesis and Sauter mean particle diameter (d_{32}) of CNT products as a function of (a) the U/U_{mf} ratio, (b) carbon source gas type, (c) the C_2H_2 ratio in the total gas feed, (d) reaction temperature, (e) H_2/C_2H_2 ratio, and (f) Ni loading.

The dash line represents the initial d_{32} of catalysts before synthesis. [Color figure can be viewed in the online issue, which is available at www.interscience.wiley.com.]

CNTs. However, we estimate the proportion of coiled CNTs to be between 5 and 10% from studying 30 TEM images. It can thus be concluded that coiled CNTs appear as a by-product in the reaction products using Ni catalysts. The appearance of coiled CNTs as a by-product was also reported by Perez-Cabero et al.[20] on Fe/Al_2O_3 in a fluidized-bed.

The TEM images in Figure 8 confirm the differential weight loss results that the quantity of amorphous carbon increases as the U/U_{mf} ratio increases up to 3, and decreases when the U/U_{mf} ratio further increases to 6, but do not help determine the oxidation behavior of coiled CNTs on which there have been no results reported in the literature. At an atomic level, straight CNTs are constructed by rolling up hexagonal graphene layers seamlessly into cylinders.[44,45] By contrast, Dunlap[46] proposed that the coiling of CNTs was caused by pentagon-heptagon pairing with the carbon matrix. Each C_5–C_7 pair is inserted into hexagonal carbon rings to form a 'knee' that connects two straight CNT sections of the same diameter. Therefore, coiled CNTs are an array of such knees.[47] It is uncertain whether the oxidation of coiled CNTs comprising C_5–C_7 pairs lies in the amorphous carbon or CNT peak range. More work is required on the oxidation behavior of coiled CNTs.

Effect of carbon source gas type

The data in Figure 4b show that the bed pressure drop increases by 1.93 and 5.97 kPa, respectively, using C_2H_4 and C_2H_2 as the carbon source. The change in the primary particle size of the reaction products as a function of carbon source (Figure 4b) and weight loss profiles of the reaction products (Figure 5c) confirm that C_2H_2 leads to a greater quantity of deposited CNTs on the catalyst particles, most likely due to its greater thermodynamic reactivity (e.g., the reactions of C_2H_2 and C_2H_4 individually with H_2 are exothermic with an enthalpy of -174.26 and -136.47 kJ). This

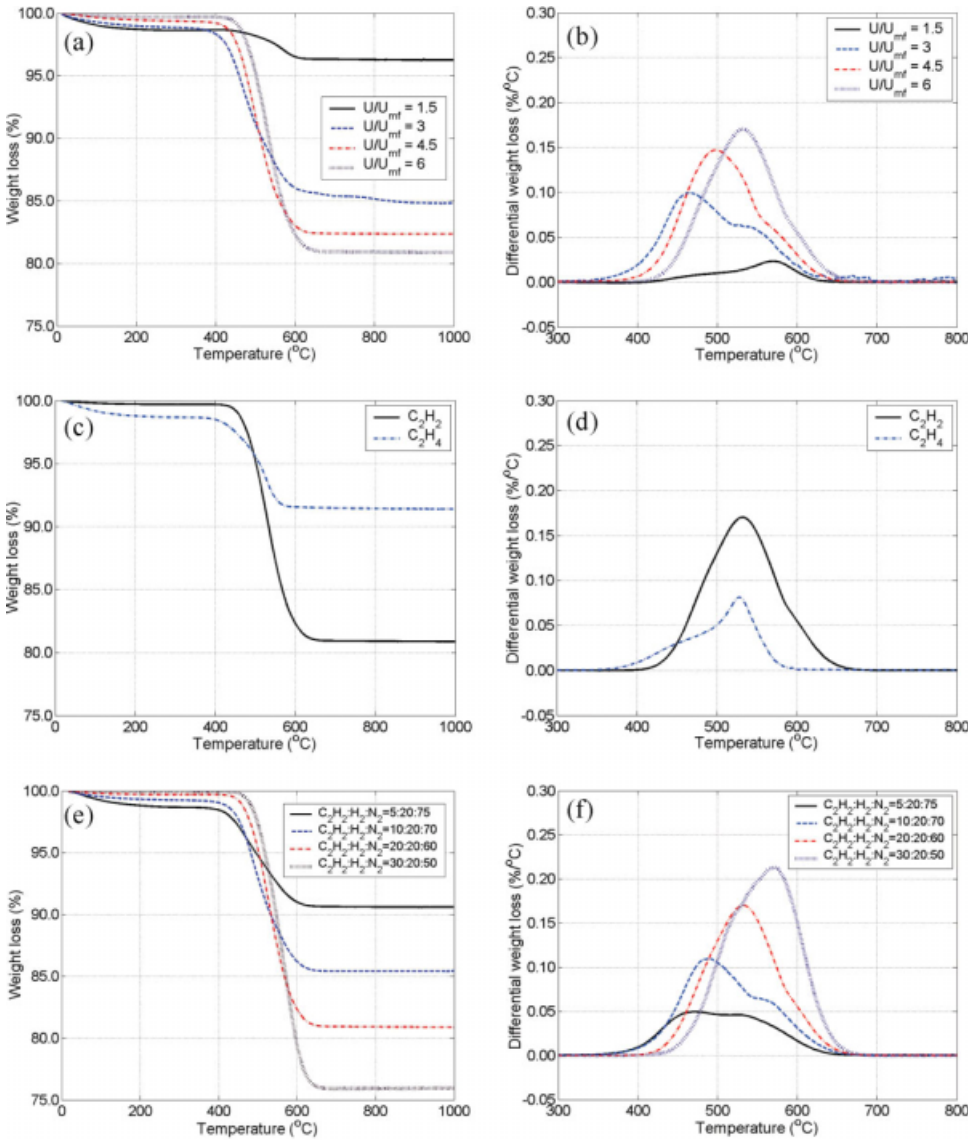

Figure 5. Thermogravimetric analysis of CNT products at various synthesis conditions: (a and b) weight loss and differential weight loss profiles for the CNT products synthesized at the U/U_{mf} of 1.5, 3, 4.5, and 6; (c and d) weight loss and differential weight loss profiles for the CNT products synthesized by C_2H_2 and C_2H_4; (e and f) weight loss and differential weight loss profiles for the CNT products synthesized in 5, 10, 20, and 30% C_2H_2 in the total gas feed; (g and h) weight loss and differential weight loss profiles for the CNT products synthesized at 650, 700, 750, and 800°C; (i and j) weight loss and differential weight loss profiles for the CNT products synthesized at the H_2/C_2H_2 ratio of 0, 0.5, 1, and 2; (k and l) weight loss and differential weight loss profiles for the CNT products synthesized on 5, 10, 20, and 40% Ni loading on Al_2O_3.

The samples were heated in air between 25 and 1000°C at a ramp rate of 5°C/min. [Color figure can be viewed in the online issue, which is available at www.interscience.wiley.com.]

in turn causes a higher bed pressure drop than for C_2H_4. This agrees with the results of Son et al.,[33] using Fe-Mo/MgO catalysts in a fluidized-bed CVD system and Hernadi et al.,[18] using Fe-based catalysts in a fixed-bed CVD system. Furthermore, the choice of carbon source is reported to influence the CNT growth.[42,48] Hernadi et al.[48] reported that C_2H_2 had higher reactivity and higher deposition rates on Fe- and Co-based catalysts than C_2H_4 in a fixed-bed system, in accordance with our results.

The differential weight loss profiles (Figure 5d) show that the quantity of amorphous carbon formed from C_2H_2 is less than that from C_2H_4, leading to a higher conversion of carbon into CNTs. This is confirmed by the Raman spectra (Figure 6a) and the I_D/I_G ratio (Figure 7a), showing that the CNT products synthesized by C_2H_2 are more highly graphitized than those from C_2H_4. This is also consistent with the work of Hernadi et al.[18] and Son et al.[33] using Fe-based catalysts.

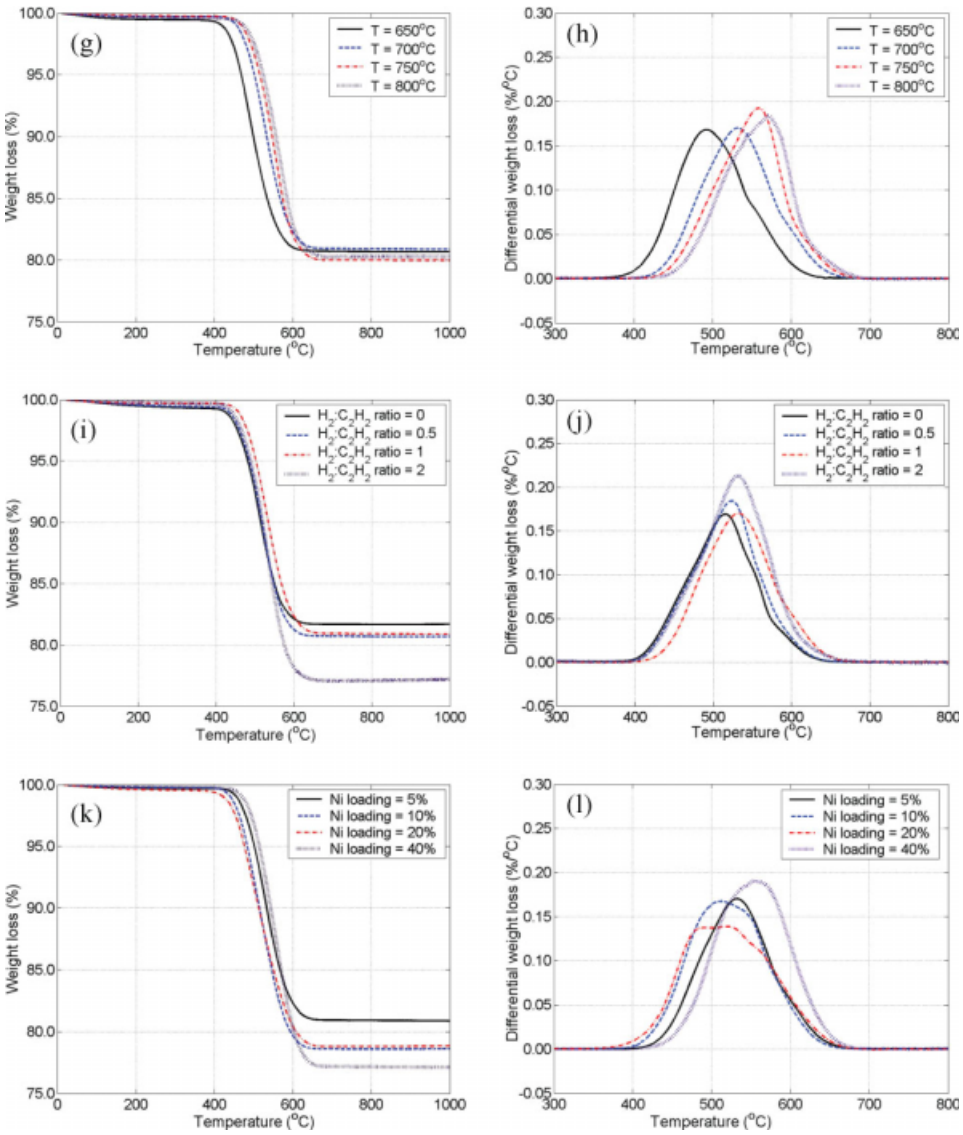

Figure 5. (Continued)

Effect of the quantity of carbon in the total gas feed

The data in Figure 4c show that the bed pressure drop increases by 2.07, 2.62, 5.97, and 12.31 kPa, for synthesis performed in 5, 10, 20, and 30% C_2H_2, respectively, in the feed gas. The increase in pressure drop as a function of the C_2H_2 ratio in the feed gas is most likely due to increased carbon availability. This is confirmed by the change in the primary particle size of the reaction products as a function of C_2H_2 ratio in the feed gas (Figure 4c) and the weight loss profiles (Figure 5e). This phenomenon was also reported by Escobar et al.[49] using Fe catalysts in a fixed bed.

As discussed earlier, carbon diffuses into active catalyst sites subsequently forming tubular structures, which cease growing when the catalyst becomes encapsulated by solid carbon.[41] Therefore, the quantity of carbon in the system is critical to the balance between the growth of CNTs and the deactivation of catalysts. When the catalyst deactivates, amorphous carbon preferentially grows from the hydrocarbon feedstock. The differential weight loss profiles (Figure 5f) show that the quantity of amorphous carbon increases as the C_2H_2 ratio in the total gas feed increases up to 10%. However, it dramatically decreases when the C_2H_2 ratio in the total gas feed exceeds 10%, suggesting that more carbon in the total gas feed leads to a greater quantity of MWNTs. This suggests that the growth rates of amorphous carbon and CNTs are competitive and depend on carbon availability. The formation of amorphous carbon is preferred as the C_2H_2 ratio in the total gas feed increases up to 10%, whereas the opposite is observed as the C_2H_2 ratio in the total gas feed exceeds 10%. This result is in contrast to Escobar et al.[49] who determined that CNT deposition increased with an increasing percentage of C_2H_2 in the gas feed between 2.5 and 10 vol % on Fe catalysts.

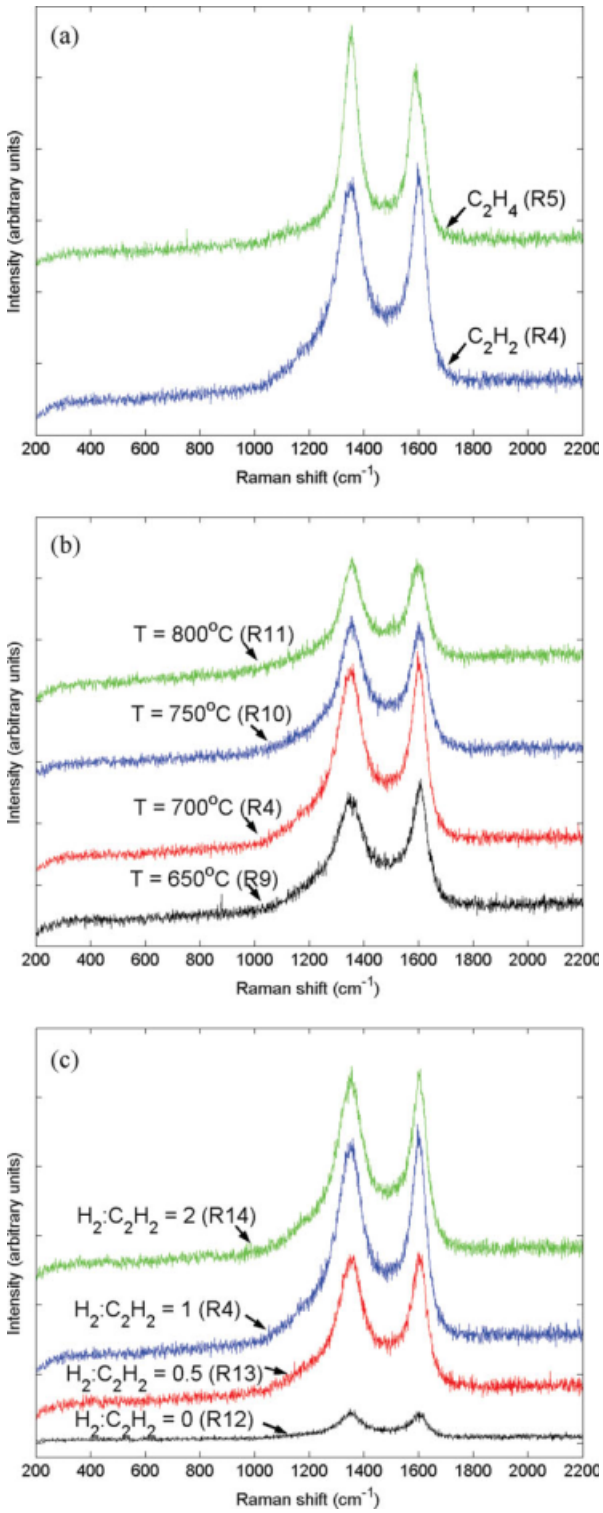

Figure 6. Raman spectra of the CNT products synthesized.

(a) by C_2H_2 and C_2H_4, (b) at 650, 700, 750, and 800°C, (c) at the H_2/C_2H_2 ratio of 0, 0.5, 1, and 2. [Color figure can be viewed in the online issue, which is available at www.interscience.wiley.com.]

Effect of reaction temperature

The data in Figure 4d show that the bed pressure drop increased by 5.17, 5.97, 4.34, and 3.93 kPa for the synthesis performed at 650, 700, 750, and 800°C, respectively. These data suggest that the increase in pressure drop across the bed is relatively independent of reaction temperature, most likely caused by the constant activity of Ni catalysts at these temperatures.[12,50] This is confirmed once again by the change in the primary particle size of the reaction products as a function of reaction temperature (Figure 4d) and weight loss

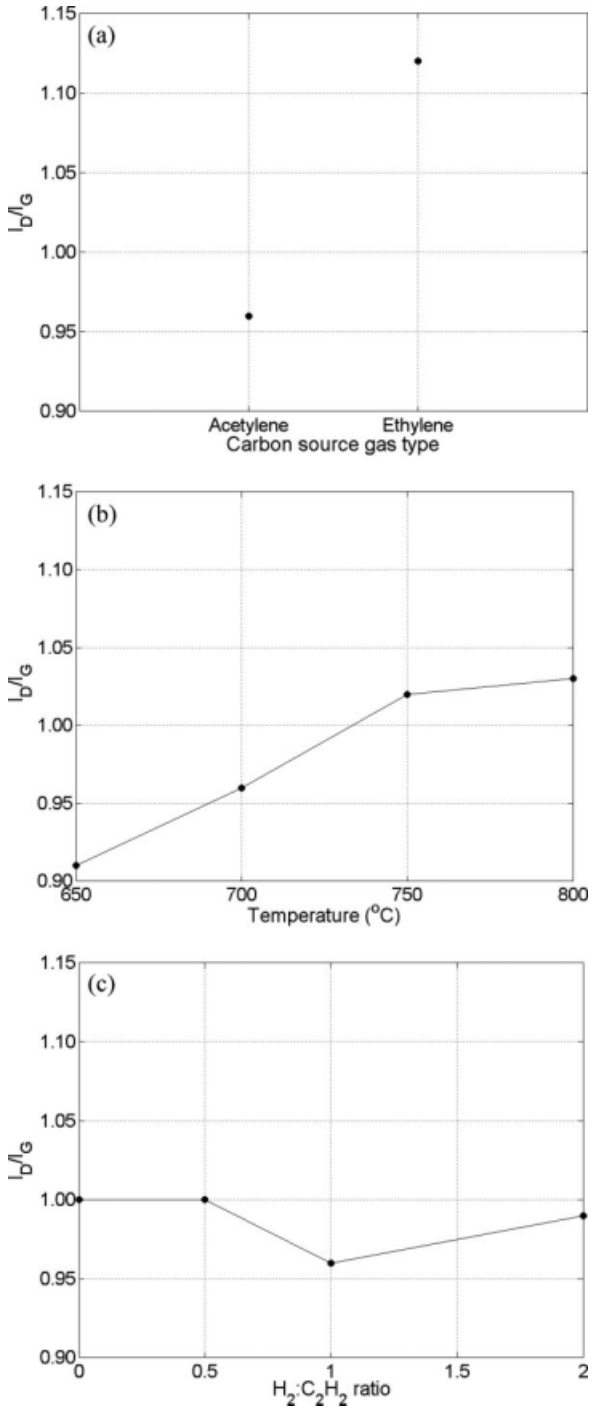

Figure 7. Ratio of D-band intensity to G-band intensity (I_D/I_G) calculated from the data in Figure 6 as a function of (a) carbon source gas type, (b) reaction temperature, and (c) the H_2/C_2H_2 ratio.

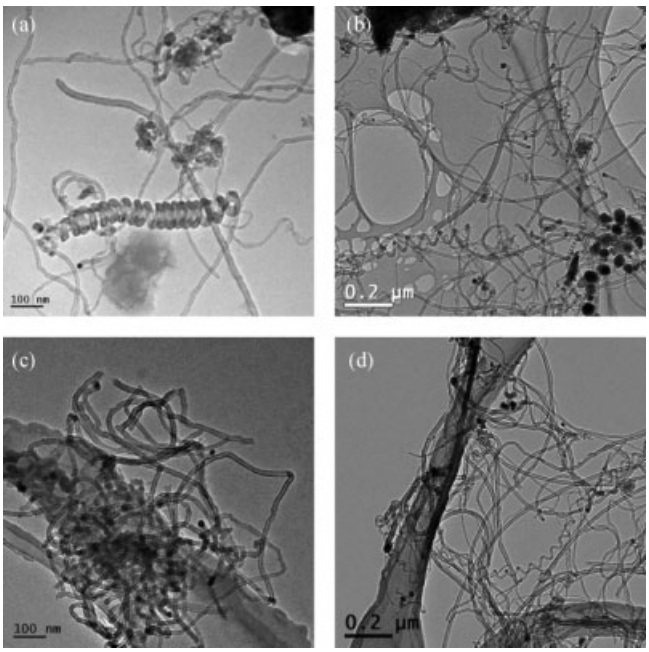

Figure 8. TEM images of CNT products at different U/U_{mf} ratio: (a) 1.5, (b) 3, (c) 4.5, and (d) 6.

The CNT products are mainly straight CNTs with a few spiral CNTs and amorphous carbon (solid black particles) as by-products. In this article, spiral CNTs refers to CNTs with a regular coiled structure.

profiles (Figure 5g) and is consistent with the work of Philippe et al.,[12] Villacampa et al.,[50] and Chen et al.[51] using Ni catalysts.

In the differential weight loss profiles (Figure 5h), the quantity of amorphous carbon is observed to increase as reaction temperature increases, likely caused by faster catalyst sintering and deactivation by carbon deposition at higher temperatures.[36] This is confirmed by the Raman spectra (Figure 6b) and the I_D/I_G ratio (Figure 7b) and agrees with results reported by Veziri et al.[36] and Cui et al.[52] In addition, in Figure 5h the mid-point of the oxidation peak appears at 500, 510, 580, and 585°C for each of the products synthesized at 650, 700, 750, and 800°C, respectively. It has been reported that increasing reaction temperatures leads to an increase in the diameter of the resultant MWMTs due to the formation of larger clusters of active metal catalysts at higher temperatures.[53,54] The peak centre appears at a higher temperature when a higher synthesis reaction temperature is used, most likely caused by the oxidization of larger diameters of MWNTs at higher temperatures.

Effect of H_2:C_2H_2 ratio

Figure 4e shows that a step change increase in the H_2/C_2H_2 ratio from 0 to 2 results in an increase in the bed pressure drop from 1.24 to 9.72 kPa. Again, the increase in the change in the primary particle size of the reaction products as a function of H_2/C_2H_2 ratio (Figure 4e) shows that a larger H_2/C_2H_2 ratio leads to a greater quantity of carbon deposited on the catalyst particles, in turn causing a higher bed pressure drop. This is confirmed by the weight loss profiles (Figure 5i) and the I_D/I_G ratio (Figure 7c) and is in agreement with Venegoni et al.[9] who showed that an increase in carbon deposition was observed when the H_2/C_2H_2 ratio was increased up to 7 on Fe/SiO_2 in a fluidized bed.

A review of the literature suggests that H_2 is essential for two aspects of the CVD synthesis of CNTs: (a) catalyst reduction and (b) kinetic balance for carbon source decomposition.[43,50,55] In the CNT growth mechanism discussed earlier, the nucleation of active sites, from which H_2 desorbs and carbon atoms dissolve into the Ni sites, forming nickel carbide (NiC).[43] However, H_2, as one of the products of C_2H_2 decomposition, has a thermodynamically reverse impact on the carbon source decomposition during CNT synthesis. Based on the impacts on both catalyst reduction and carbon source decomposition reaction, the ratio of H_2 to C_2H_2 is one of the most influential variables investigated in this study. The bed pressure drop (Figure 4e), the change in the primary particle size of the reaction products as a function of H_2:C_2H_2 ratio (Figure 4e) and the weight loss profiles (Figure 5i) suggest that the increase in the H_2:C_2H_2 ratio up to 2 causes an increase in reduced, i.e., Ni(0) sites of active catalyst, in turn leading to increased CNT formation. The inhibiting impact on carbon source decomposition is macroscopically negligible in this case.

In the differential weight loss profiles (Figure 5j), the absence of an amorphous carbon subpeak or shoulder between 300 and 500°C suggests that little amorphous carbon exists in the reaction products. In addition, little difference is observed in the differential weight loss profiles as the H_2:C_2H_2 ratio increases, suggesting that the H_2/C_2H_2 ratio has no impact on the ratio of amorphous carbon to CNTs in the fluidized-bed CVD system. This is in contrast to Donato et al.[37] who suggested that increased $[H_2]$ decreases the growth of amorphous carbon in the CNT products on Fe catalyst using C_2H_6 as carbon source in a fixed-bed CVD system.

Effect of Ni loading

Figure 4f shows that the increase in pressure drop across the bed is comparatively insensitive to the nickel loading. This is confirmed once again by the change in the primary particle size of the reaction products as a function of nickel loading (Figure 4f) and the weight loss profiles measured using TGA (Figure 5k) which show that the total weight loss for the CNT products synthesized on 5, 10, 20, and 40% Ni loadings on Al_2O_3 is 19.3, 21.2, 21.5, and 22.8%, respectively. This result appears inconsistent with the results reported by Ermakova et al.[24] who showed that an increase in the Ni loading from 30 to 96 wt % led to an increase in the carbon yield from 120 to 238 g carbon/g Ni, i.e., the more Ni loading on catalyst supports lead to more carbon deposited.

In the differential weight loss profiles (Figure 5l), the peaks at 510, 500, 500, and 560°C are observed for the CNT product synthesized on 5, 10, 20, and 40% Ni loadings, respectively. Little difference in the peak as increasing Ni loading up to 20% is most likely caused by the oxidization of MWNTs of similar diameter. However, the peak shifts 50°C higher when Ni loading exceeds 20%, most likely due to the oxidization of large-sized MWNTs.[56] It has been reported that CNT diameter depends largely upon the size of

Table 2. Summary of the Carbon Deposition, CNT Yield, and CNT Selectivity for the Fluidized-Bed Products

Run	Carbon Deposition (wt %)	CNT Purity (wt %)	CNT Selectivity (%)
R1	3.8	1.8	47.4
R2	15.1	6.7	44.4
R3	17.5	9.1	52.0
R4	18.4	13.4	72.8
R5	8.1	3.1	38.3
R6	9.2	3.9	42.4
R7	14.7	7.2	49.0
R8	23.9	21.3	89.1
R9	19.2	9.1	47.4
R10	20.0	17.5	87.5
R11	19.7	17.5	88.8
R12	17.9	10.2	57.0
R13	19.4	11.7	60.3
R14	22.7	15.0	66.1
R15	21.3	16.4	77.0
R16	21.0	13.3	63.3
R17	22.6	14.9	65.9

In experiments R1–R4, the influence of the U/U_{mf} ratio was studied (1.5, 3, 4.5, or 6, respectively); in R4 and R5, the carbon source gas was changed from C_2H_2 to C_2H_4, whereas in R6, R7, R4, and R8, the C_2H_2 ratio in the total gas feed was studied (at 5, 10, 20, or 30%, respectively). In R9, R4, R10, and R11, the reaction temperature (650, 700, 750, or 800°C, respectively), in R12, R13, R4, and R14, the H_2/C_2H_2 ratio (0, 0.5, 1, or 2, respectively), and in R4, R15, R16, and R17, the Ni loading (5, 10, 20, or 40%, respectively).

catalyst particles.[57,58] The Ni loading beyond 20% most likely leads to the formation of Ni active sites of large surface area on the Al_2O_3 powders which activate the growth of MWNTs in large diameter. This agrees with the results of Ermakova et al.[24] that more Ni loading results in the formation of large size of metal catalysts.

Table 2 shows the summary of carbon deposition, CNT yield and CNT selectivity for the fluidized-bed products. From Figure 5, carbon deposition and CNT yield were inferred from the weight loss from 300 to 700°C and from 500 to 700°C, respectively. The CNT selectivity is determined by CNT yield divided by carbon deposition. The optimized conditions were found to be R8 in which the MWNT synthesis was performed in the mixture of C_2H_2:H_2:N_2 in the volume ratio of 30:20:50 on 5% Ni/Al_2O_3 at 700°C for 30 min. Under such conditions, carbon deposition, CNT yield and CNT selectivity reached the highest, i.e., 23.9, 21.3, and 89.1 wt %, respectively. However, it is worth mentioning that the reaction products are a mixture of MWNTs, Ni, Al_2O_3 and by-products, e.g., amorphous carbon. Further purification is required to obtain high-purity CNTs for end use.

Conclusions

A systematic study of the synthesis of MWNTs on Ni/Al_2O_3 catalysts from C_2H_2 and C_2H_4 feedstocks has been undertaken. The effects of: (a) U/U_{mf}, (b) carbon source gas type, (c) C_2H_2 ratio in the total feed gas, (4) reaction temperature, (5) H_2/C_2H_2 ratio, and (6) Ni loading on Al_2O_3 have been studied. The pressure drop across the fluidized-bed increases as reaction time increases, and as U/U_{mf} and the carbon ratio in the total feed gas increase, but is largely independent of reaction temperature and Ni loading. The particle size of the reaction products and TGA weight loss results confirm the bed pressure drop measurements. The deposition of MWNTs on catalyst particles results in substantial changes to the depth and structure of the fluidized bed as the reaction proceeds, in turn significantly altering the bed hydrodynamics. TEM images of the bed materials show that MWNTs, metal catalysts and alumina supports were predominant in the product mixture, with coiled CNTs as a by-product.

Acknowledgments

J.L. is grateful to the School of Chemical and Biomolecular Engineering at the University of Sydney for a Postgraduate Research Scholarship. The authors are grateful to Dr. I. Kaplin in the University's Electron Microscopy Unit for assistance with the operation of the SEM and Dr. E. Carter in the School of Chemistry for assistance with Raman spectroscopy measurements.

Literature Cited

1. Li F, Zhu ZG, Yao XD, Lu GQ, Zhao MW, Xia YY, Chen Y. Fluorination-induced magnetism in boron nitride nanotubes from ab initio calculations. *Appl Phys Lett*. 2008;92:102515-1–102512-3.
2. Chen K-C, Chen C-F, Lee J-H, Wu T-L, Hwang C-L, Tai N-H, Hsiao M-C. Low-temperature CVD growth of carbon nanotubes for field emission application. *Diamond Relat Mater*. 2007;16:566–569.
3. Tkac J, Whittaker JW, Ruzgas T. The use of single walled carbon nanotubes dispersed in a chitosan matrix for preparation of a galactose biosensor. *Biosens Bioelectron*. 2007;22:1820–1824.
4. Okuyama H, Iwata N, Yamamoto H. Position-selective growth of vertically aligned carbon nanotubes for application of electronic-measuring nanoprobes. *Phys E: Low-dimensional Syst Nanostruct*. 2007;37:49–53.
5. Iijima S, Wakabayashi T, Achiba Y. Structures of carbon soot prepared by laser ablation. *J Phys Chem*. 1996;100:5839–5843.
6. Ebbesen TW, Ajayan PM. Large-scale synthesis of carbon nanotubes. *Nature*. 1992;358:220–222.
7. Joseyacaman M, Mikiyoshida M, Rendon L, Santiesteban JG. Catalytic growth of carbon microtubules with fullerene structure. *Appl Phys Lett*. 1993;62:657–659.
8. Dal HJ, Rinzler AG, Nikolaev P, Thess A, Colbert DT, Smalley RE. Single-wall nanotubes produced by metal-catalyzed disproportionation of carbon monoxide. *Chem Phys Lett*. 1996;260:471–475.
9. Venegoni D, Serp P, Feurer R, Kihn Y, Vahlas C, Kalck P. Parametric study for the growth of carbon nanotubes by catalytic chemical vapor deposition in a fluidized bed reactor. *Carbon*. 2002;40:1799–1807.
10. Wang Y, Wei F, Gu GS, Yu H. Agglomerated carbon nanotubes and its mass production in a fluidized-bed reactor. *Phys B: Condens Matter*. 2002;323:327–329.
11. See CH, Harris AT. A review of carbon nanotube synthesis via fluidized-bed chemical vapor deposition. *Ind Eng Chem Res*. 2007;46:997–1012.
12. Philippe R, Moranqais A, Corrias M, Caussat B, Kihn Y, Kalck P, Plee D, Gaillard P, Bernard D, Serp P. Catalytic production of carbon nanotubes by fluidized-bed CVD. *Chem Vapor Deposition*. 2007;13:447–457.
13. Weidenkaff A, Ebbinghaus SG, Mauron P, Reller A, Zhang Y, Zuttel A. Metal nanoparticles for the production of carbon nanotube composite materials by decomposition of different carbon sources. *Mater Sci Eng Biomim Supramol Syst*. 2002;19:119–123.
14. Corrias M, Caussat B, Ayral A, Durand J, Kihn Y, Kalck P, Serp P. Carbon nanotubes produced by fluidized bed catalytic CVD: first approach of the process. *Chem Eng Sci*. 2003;58:4475–4482.
15. Morancais A, Caussat B, Kihn Y, Kalck P, Plee D, Gaillard P, Bernard D, Serp P. A parametric study of the large scale production of multi-walled carbon nanotubes by fluidized bed catalytic chemical vapor deposition. *Carbon*. 2007;45:624–635.
16. Wang Y, Wei F, Luo GH, Yu H, Gu GS. The large-scale production of carbon nanotubes in a nano-agglomerate fluidized-bed reactor. *Chem Phys Lett*. 2002;364:568–572.

17. Hao Y, Zhang QF, Wei F, Qian WZ, Luo GH. Agglomerated CNTs synthesized in a fluidized bed reactor: agglomerate structure and formation mechanism. *Carbon*. 2003;41:2855–2863.
18. Hernadi K, Fonseca A, Nagy JB, Bernaerts D, Lucas AA. Fe-catalyzed carbon nanotube formation. *Carbon*. 1996;34:1249–1257.
19. Qian WZ, Liu T, Wei F, Wang ZW, Li YD. Enhanced production of carbon nanotubes: combination of catalyst reduction and methane decomposition. *Appl Catal A Gen*. 2004;258:121–124.
20. Perez-Cabero M, Rodriguez-Ramos I, Guerrero-Ruiz A. Characterization of carbon nanotubes and carbon nanofibers prepared by catalytic decomposition of acetylene in a fluidized bed reactor. *J Catal*. 2003;215:305–316.
21. Ago H, Uehara N, Yoshihara N, Tsuji M, Yumura M, Tomonaga N, Setoguchi T. Gas analysis of the CVD process for high yield growth of carbon nanotubes over metal-supported catalysts. *Carbon*. 2006;44:2912–2918.
22. Mauron P, Emmenegger C, Sudan P, Wenger R, Rentsch S, Zuttel A. Fluidised-bed CVD synthesis of carbon nanotubes on Fe_2O_3/MgO. *Diamond Relat Mater*. 2003;12:780–785.
23. Li YL, KinlochIA, Shaffer MS, Geng JF, Johnson B, Windle AH. Synthesis of single-walled carbon nanotubes by a fluidized-bed method. *Chem Phys Lett*. 2004;384:98–102.
24. Ermakova MA, Ermakov DY, Kuvshinov GG, Plyasova LM. New nickel catalysts for the formation of filamentous carbon in the reaction of methane decomposition. *J Catal*. 1999;187:77–84.
25. Qian WH, Liu TA, Wang ZW, Wei FA, Li ZF, Luo GH, Li YD. Production of hydrogen and carbon nanotubes from methane decomposition in a two-stage fluidized bed reactor. *Appl Catal A Gen*. 2004;260:223–228.
26. Kibria A, Mo YH, Nahm KS, Kim MJ. Synthesis of narrow-diameter carbon nanotubes from acetylene decomposition over an iron-nickel catalyst supported on alumina. *Carbon*. 2002;40:1241–1247.
27. McAuley KB, Talbot JP, Harris TJ. A comparison of 2-phase and well-mixed models for fluidized-bed polyethylene reactors. *Chem Eng Sci*. 1994;49:2035–2045.
28. Wang XS, Palero V, Soria J, Rhodes MJ. Laser-based planar imaging of nano-particle fluidization. I. Determination of aggregate size and shape. *Chem Eng Sci*. 2006;61:5476–5486.
29. Müller,U, Hauert R, Oral B, Tobler M. Pores in hydrogenated amorphous carbon films on stainless steel. *Surf Coat Technol*. 1995;71:233–238.
30. Baba K, Hatada R. Preparation of amorphous carbon thin films by ion beam assisted ECR-plasma CVD. *Nucl Instrum Methods Phys Res Sect B*. 1997;121:129–132.
31. Qian WZ, Wei F, Wang ZW, Liu T, Yu H, Luo GH, Xiang L, Deng XY. Production of carbon nanotubes in a packed bed and a fluidized bed. *AIChE J*. 2003;49:619–625.
32. See CH, Harris AT. On the development of fluidized bed chemical vapour deposition for large-scale carbon nanotube synthesis: influence of synthesis temperature. *Aust J Chem*. 2007;60:541–546.
33. Son SY, Lee Y, Won S, Lee DH, Kim SD, Sung SW. High-quality multiwalled carbon nanotubes from catalytic decomposition of carboneous materials in gas-solid fluidized beds. *Ind Eng Chem Res*. 2008;47:2166–2175.
34. Xu CB, Zhu J. One-step preparation of highly dispersed metal-supported catalysts by fluidized-bed MOCVD for carbon nanotube synthesis. *Nanotechnology*. 2004;15:1671–1681.
35. McKee GSB, Vecchio KS. Thermogravimetric analysis of synthesis variation effects on CVD generated multiwalled carbon nanotubes. *J Phys Chem B*. 2006;110:1179–1186.
36. Veziri CM, Pilatos G, Karanikolos GN, Labropoulos A, Kordatos K, Kasselouri-Rigopoulou V, Kanellopouios NK. Growth and optimization of carbon nanotubes in activated carbon by catalytic chemical vapor deposition. *Microporous Mesoporous Mater*. 2008;110:41–50.
37. Donato MG, Messina G, Milone C, Pistone A, Santangelo S. Experiments on C nanotubes synthesis by Fe-assisted ethane decomposition. *Diamond Relat Mater*. 2008;17:318–324.
38. Mori S, Suzuki M. Effect of oxygen and hydrogen addition on the low-temperature synthesis of carbon nanofibers using a low-temperature CO/Ar DC plasma. *Diamond Relat Mater*. 2008;17:999–1002.
39. Liu QX, Fang Y. New technique of synthesizing single-walled carbon nanotubes from ethanol using fluidized-bed over Fe-Mo/MgO catalyst. *Spectrochim Acta Part A*. 2006;64:296–300.
40. Liu J, Harris AT. Microwave-assisted acid digestion of alumina-supported carbon nanotubes. *Sep Purif Technol*. 2008;62:602–608.
41. Baker RTK, Barber MA, Waite RJ, Harris PS, Feates FS. Nucleation and growth of carbon deposits from nickel catalyzed decomposition of acetylene. *J Catal*. 1972;26:51–62.
42. Teo KBK, Chhowalla M, Milne WI. Catalytic synthesis of carbon nanotubes and nanofibers. *Enc. of Nanosci. and Nanotech*. 2003;X:1–22.
43. De Jong KP, Geus JW. Carbon nanofibers: catalytic synthesis and applications. *Catal Rev—Sci Eng*. 2000;42:481–510.
44. Iijima S. Helical microtubules of graphitic carbon. *Nature*. 1991;354:56–58.
45. Iijima S, Ichihashi T. Single-shell carbon nanotubes of 1-nm diameter. *Nature*. 1993;363:603–605.
46. Dunlap BI. Constraints on small graphitic helices. *Phys Rev B*. 1994;50:8134–8137.
47. Dunlap BI. Relating carbon tubules. *Phys Rev B*. 1994;49:5643–5650.
48. Hernadi K, Fonseca A, Nagy A, Siska A, Kiricsi I. Production of nanotubes by the catalytic decomposition of different carbon-containing compounds. *Appl Catal A*. 2000;199:245–255.
49. Escobar M, Moreno MS, Candal RJ, Marchi MC, Caso A, Polosecki PI, Rubiolo GH, Goyanes S. Synthesis of carbon nanotubes by CVD: effect of acetylene pressure on nanotubes characteristics. *Appl Surf Sci*. 2007;254:251–256.
50. Villacampa JI, Royo C, Romeo E, Montoya JA, Del Angel P, Monzon A. Catalytic decomposition of methane over Ni-A1203 coprecipitated catalysts reaction and regeneration studies. *Appl Catal A*. 2003;252:363–383.
51. Chen D, Christensen KO, Ochoa-Fernandez E, Yu ZX, Totdal B, Latorre N, Monzon A, Holmen A. Synthesis of carbon nanofibers: effects of Ni crystal size during methane decomposition. *J Catal*. 2005;229:82–96.
52. Cui H, Eres G, Howe JY, Puretkzy A, Varela M, Geohegan DB, Lowndes DH. Growth behavior of carbon nanotubes on multilayered metal catalyst film in chemical vapor deposition. *Chem Phys Lett*. 2003;374:222–228.
53. Singh C, Shaffer MS, Windle AH. Production of controlled architectures of aligned carbon nanotubes by an injection chemical vapour deposition method. *Carbon*. 2003;41:359–368.
54. Sampedro-Tejedor P, Maroto-Valiente A, Nevskaia DM, Munoz V, Rodriguez-Ramos I, Guerrero-Ruiz A. The effect of growth temperature and iron precursor on the synthesis of high purity carbon nanotubes. *Diamond Relat Mater*. 2007;16:542–549.
55. Piao LY, Li YD, Chen JL, Chang L, Lin JYS. Methane decomposition to carbon nanotubes and hydrogen on an alumina supported nickel aerogel catalyst. *Catal Today*. 2002;74:145–155.
56. Zhang HY, Chen YM, Zeng GX, Huang HP, Xie ZW, Jie XH. The thermal properties of controllable diameter carbon nanotubes synthesized by using AB(5) alloy of micrometer magnitude as catalyst. *Mater Sci Eng A*. 2007;464:17–22.
57. Li YM, Kim W, Zhang YG, Rolandi M, Wang DW, Dai HJ. Growth of single-walled carbon nanotubes from discrete catalytic nanoparticles of various sizes. *J Phys Chem B*. 2001;105:11424–11431.
58. Cheung CL, Kurtz A, Park H, Lieber CM. Diameter-controlled synthesis of carbon nanotubes. *J Phys Chem B*. 2002;106:2429–2433.

Manuscript received Sept. 13, 2008, revision received Mar. 22, 2009, and final revision received May 13, 2009.